

Metal Soap Membranes for Gas Separation

Qi Liu, Deepu J. Babu, Jian Hao, Mohammad Tohidi Vahdat, Davide Campi, and Kumar Varoon Agrawal*

Metal soaps or metal alkanoates are metal–organic complexes held together with metal cations and the functional groups of hydrocarbon chains. They can be synthesized at a high yield by simply mixing the metal and organic sources, forming crystalline frameworks with diverse topology, and have been studied in the past because of their rich polymorphism-like liquid crystals. Their ability to melt while retaining the crystalline properties upon cooling is unique among nanoporous materials and is especially attractive for membrane fabrication. Herein, metal soaps as a new class of material for molecular separation are reported. Three metal soaps, $\text{Ca}(\text{SO}_4\text{C}_{12}\text{H}_{25})_2$, $\text{Zn}(\text{COOC}_6\text{H}_{13})_2$, and $\text{Cu}(\text{COOC}_9\text{H}_{19})_2$, hosting lamellar structure with molecular-sized channels are synthesized. They are processed in thin, intergrown, polycrystalline films on porous substrates by two scalable methods, interfacial crystallization and melting with an extremely small processing time (a minute to an hour). The resulting crystalline films are oriented with the alkyl chains perpendicular to the porous substrate which favors molecular transport. The prepared membranes demonstrate attractive gas separation behavior, e.g., 300-nm-thick $\text{Ca}(\text{SO}_4\text{C}_{12}\text{H}_{25})_2$ membrane prepared in a minute using interfacial crystallization yields H_2 permeance of $6.1 \times 10^{-7} \text{ mol m}^{-2} \text{ s}^{-1} \text{ Pa}^{-1}$ with H_2/CO_2 selectivity of 10.5.

1. Introduction

Molecular separation using membranes is highly energy-efficient because the driving force for separation does not rely on the relatively expensive thermal energy but on the chemical potential difference across the membranes.^[1–9] Several materials and chemistries have been used to develop the selective layer of the membranes, including polymers,^[2,7,10,11] carbon,^[12–14] zeolites,^[1,15,16] and more recently, metal–organic frameworks (MOFs)^[4,17–22] and covalent–organic frameworks (COFs).^[23–27] One of the most sought-after strategies to develop the selective

layer is to advance the material chemistry and engineering such that one can obtain a good separation performance (a combination of gas permeance and gas pair selectivity), while at the same time, can process the material in a scalable way. For example, polymers are predominately used as the selective material for membranes because they are highly processible. Rigid nanoporous materials with ordered pores such as zeolite, MOFs, and COFs have been successfully used to form the selective layer with improved performance, however, one compromises the processability. Typically, to obtain an attractive performance from these materials, one has to crystallize an intergrown polycrystalline film. However, to synthesize high-quality nanoporous membranes, generally, one needs to reduce the density of pinholes and grain-boundary defects which often require time-consuming complex steps. In this regard, the synthesis of gas-selective, nanoporous, crystalline materials that can be readily processed into high-quality thin

films by scalable approaches is greatly desired.^[28]

Metal soaps or metal alkanoates, well-known by their rich polymorphism and polymesomorphism, have been used as a barrier coating,^[29–34] thermotropic ionic liquid crystals,^[35] nonlinear-optical materials,^[29] etc.^[36–39] They are constructed by predominantly inorganic bonding between metal cations (Li^+ , Na^+ , K^+ , Cs^+ , Mg^{2+} , Ca^{2+} , Sr^{2+} , Ba^{2+} , Zn^{2+} , Cu^{2+} , Cd^{2+} , Co^{2+} , Ni^{2+} , Y^{3+} , Tb^{3+} , etc.) and the functional head group (carboxylate ($-\text{COOH}$), sulfite ($-\text{SO}_3\text{H}$), sulfate ($-\text{SO}_4\text{H}$), etc.) of a hydrocarbon chain (alkyl, enyl, aryl, etc., with carbon number > 3). The resulting M–O bonds are thermally and chemically robust making metal soaps attractive for practical applications. The MO_x polyhedra form a layer of rods/chains or sheets that are sandwiched between the layers of lipidic hydrocarbon chains, leading to a lamellar structure (Figure 1 and Figure S1, Supporting Information). As early as the 1960s, Luzzati et al. reported the crystal structure of alkaline earth metal soaps by X-ray diffraction (XRD) where they revealed the ordered arrangements of metal cations and correlated the lattice parameters with the length of the hydrocarbon chain.^[40]

Due to the high flexibility of the long alkyl chains in the structures, most metal soaps can melt at a moderate temperature (100–200 °C), forming a disordered/amorphous liquid phase or a mesophase, which was first discovered back in 1855.^[35] The liquid phase can be readily cooling down, upon

Dr. Q. Liu, Dr. D. J. Babu, Dr. J. Hao, M. T. Vahdat, Prof. K. V. Agrawal
 Laboratory of Advanced Separations (LAS)
 École Polytechnique Fédérale de Lausanne (EPFL)
 Sion CH-1950, Switzerland
 E-mail: kumar.agrawal@epfl.ch

M. T. Vahdat, Dr. D. Campi
 Theory and Simulation of Materials (THEOS) and National Centre for
 Computational Design and Discovery of Novel Materials (MARVEL)
 EPFL
 Lausanne CH-1015, Switzerland

 The ORCID identification number(s) for the author(s) of this article can be found under <https://doi.org/10.1002/adfm.202005629>.

DOI: 10.1002/adfm.202005629

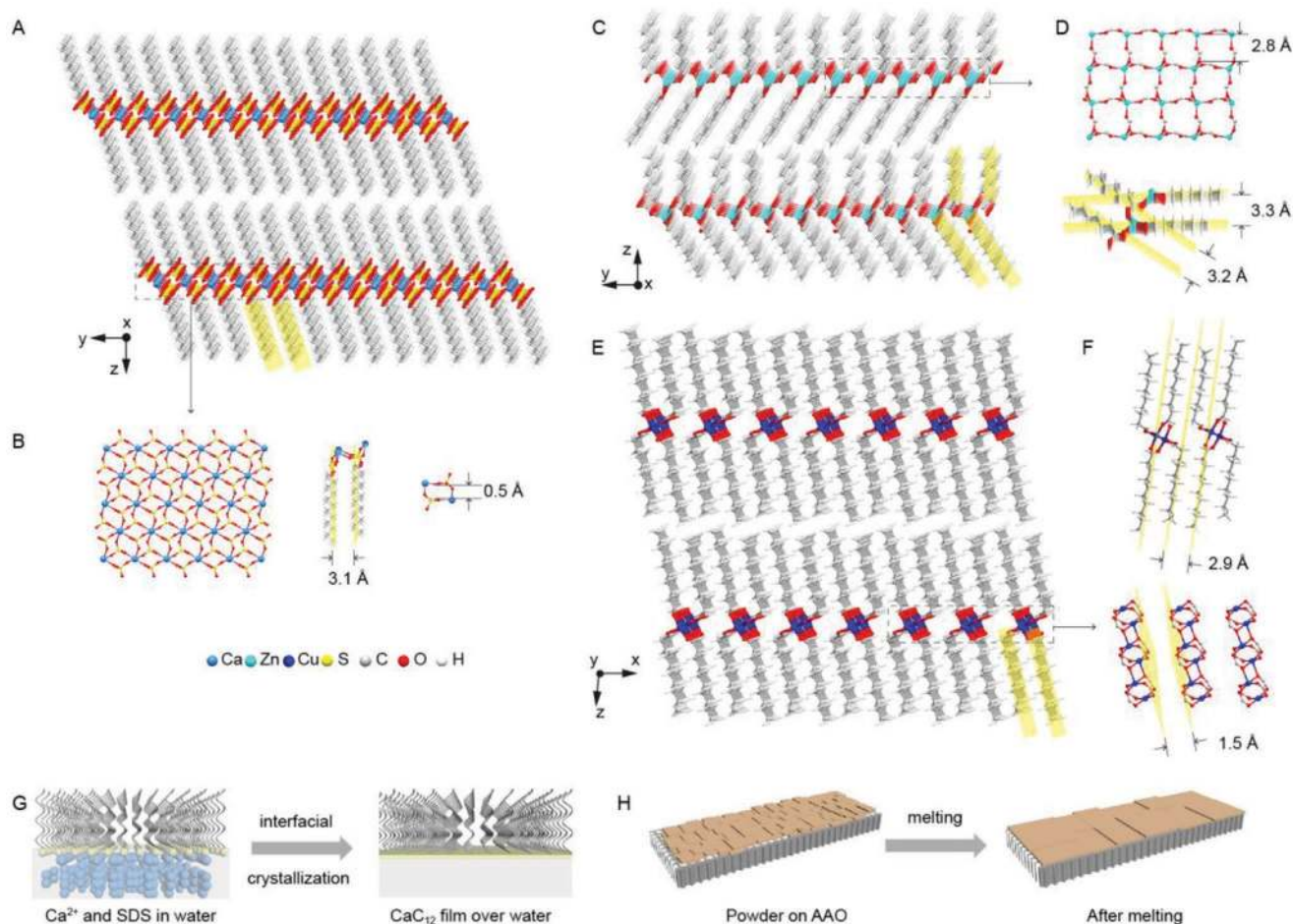


Figure 1. A) Crystal structure of CaC_{12} . B) Structure of the 2D layer and pore sizes in CaC_{12} . C) Crystal structure of ZnC_6 . D) Structure of the 2D layer and pore sizes in ZnC_6 . E) Crystal structure of CuC_9 . F) Structure of the 1D rods and pore sizes in CuC_9 . G) Scheme of CaC_{12} membrane formed by interfacial crystallization. H) Schematic of ZnC_6 and CuC_9 membranes formed by the melting.

which, the disordered structure quickly turn back to the original crystalline state. Because of the hydrophobicity of the long alkyl chains, metal soaps have been used as a “green” corrosion barrier by constructing metal soaps on the surface of metals.^[31] They also play an important role in analytical and preparative science as a means to reduce surface tension, for example, to unfold highly ordered macromolecules such as proteins.^[33] Besides, due to the high polarization between metal cations and lipidic chains during melting, metal soaps have been proved to be attractive as a nonlinear-optical material.^[31]

To the best of our knowledge, molecular separation using metal soaps has not been reported. This presents an opportunity to evaluate this class of material for the preparation of gas separation membranes especially in the context of a large number of ordered porous metal soaps that could allow separation of several gas pairs. They are particularly attractive for membranes because the synthesis of metal soap is facile, and most of them crystallize rapidly in sufficiently high yields in aqueous solutions when the reactants (metal and organic sources) are mixed. Additionally, they provide processability advantage as one could synthesize the selective layer of a membrane (thin films) by exploiting the

solid-to-liquid transition ability of metal soaps and the fact that they do not lose crystallinity upon cooling down. Finally, the melting property could also be used in the postsynthetic healing of pinhole defects that often ruin the membrane selectivity, by simply annealing the film near the melting temperature.

Herein, three metal soaps, $\text{Ca}(\text{SO}_4\text{C}_{12}\text{H}_{25})_2$, $\text{Zn}(\text{COOC}_6\text{H}_{13})_2$, and $\text{Cu}(\text{COOC}_9\text{H}_{19})_2$, termed henceforth as CaC_{12} , ZnC_6 , and CuC_9 , respectively, are synthesized in polycrystalline thin film morphology, loaded on porous supports, by two scalable methods: interfacial crystallization and melting. In the case of interfacial crystallization, a continuous film is formed on the surface of the water within 1 min, following which the film could be easily transferred to porous substrates. In the case of the melting method, the membranes were formed by melting a layer of deposited metal soap crystals at 120–150 °C in less than 1 h. The resulting films are crystalline and are oriented on the porous support with the alkyl chains perpendicular to the substrates, favoring the molecular transport. Because of the large grain size in these films (extending to several micrometers), all membranes show promising gas separation properties.

2. Results and Discussion

2.1. Crystal Structure of Metal Soaps

Metal soaps are composed of two parts: a metal cation part and an organic part. The metal cations and the functional groups from the organic part form an inorganic backbone while the long alkyl chains attached to the backbone form a lamellar structure (Figure 1 and Figure S1, Supporting Information). For example, CaC_{12} has a 2D structure where the Ca^{2+} ions are bonded with the sulfate groups from sodium dodecyl sulfate (SDS) and form a 2D backbone, while dodecyl groups from SDS are located on both sides of the 2D layer (Figure 1A,B).^[41] There are two distinct channels in CaC_{12} : one comprising of gaps between the dodecyl groups with the size of ≈ 3.1 Å (the sizes were measured by calculating the shortest distances in the gap and subtracting the radii of the edge atoms), and the other inside the four-membered inorganic ring made of Ca^{2+} /sulfate groups with a size of ≈ 0.5 Å (Figure 1B). The crystal structure of ZnC_6 is similar to CaC_{12} (Figure 1C).^[42] Zn^{2+} and carboxylate groups from heptanoic acid form a 2D backbone, with hexyl groups from heptanoic acid presenting in both sides of the layer, albeit with an asymmetric arrangement. The channel sizes between hexyl groups on the two sides of the 2D layer are ≈ 3.2 and 3.3 Å (Figure 1D). The pore size of the four-membered ring made of Zn^{2+} /carboxylate groups is ≈ 2.8 Å. In contrast, CuC_9 has a 1D structure where a rod is formed by bonding of Cu^{2+} with the carboxylate groups of decanoic acid (Figure 1E), and nonadecyl groups extend away from the rod.^[37] The channel formed between the gaps of the nonadecyl groups are ≈ 2.9 Å in size (Figure 1F). The channel between Cu^{2+} /carboxylate rods is impermeable with a size of 1.5 Å.

2.2. Synthesis of Metal Soap Membranes

CaC_{12} membranes were synthesized by the interfacial crystallization route (Figure 1G). During the synthesis of CaC_{12} powders, we noticed that a film was formed on the water surface spontaneously when the two reactants (SDS and calcium nitrate) were mixed (Video S1, Supporting Information, and Figure 2A). This gave us a clue to synthesize CaC_{12} membranes by the interfacial crystallization route because one can prepare the membrane by simply lifting off the floating film. ZnC_6 and CuC_9 did not form a film at the air–water interface. Even when the surfactant chain length was increased to up to 17 (e.g., CuC_{11} , CuC_{17} , Figure S6, Supporting Information), we did not observe interfacial crystallization. Therefore, ZnC_6 and CuC_9 membranes were synthesized by the melting route attributing to the unique melting properties of these metal soaps (Figure 1H).

For the synthesis of CaC_{12} membrane, SDS was added dropwise into the calcium nitrate aqueous solution (see the Experimental Section). Because of its amphiphilic nature, SDS forms a film on the water surface. The sulfate groups of SDS reacted immediately with Ca^{2+} in the solution, forming a CaC_{12} film covering the whole water surface (Figure 2A and Video S1, Supporting Information). The defects in the floating film were quickly healed by the spontaneous reaction, and once the film formation was complete (usually in less than 1 min), the final membrane was obtained by scooping the film with a porous substrate. Because of the flexibility of the process, we could use a number of porous supports such as porous polytetrafluoroethylene (PTFE), metal mesh, and anodic aluminum oxide (AAO).

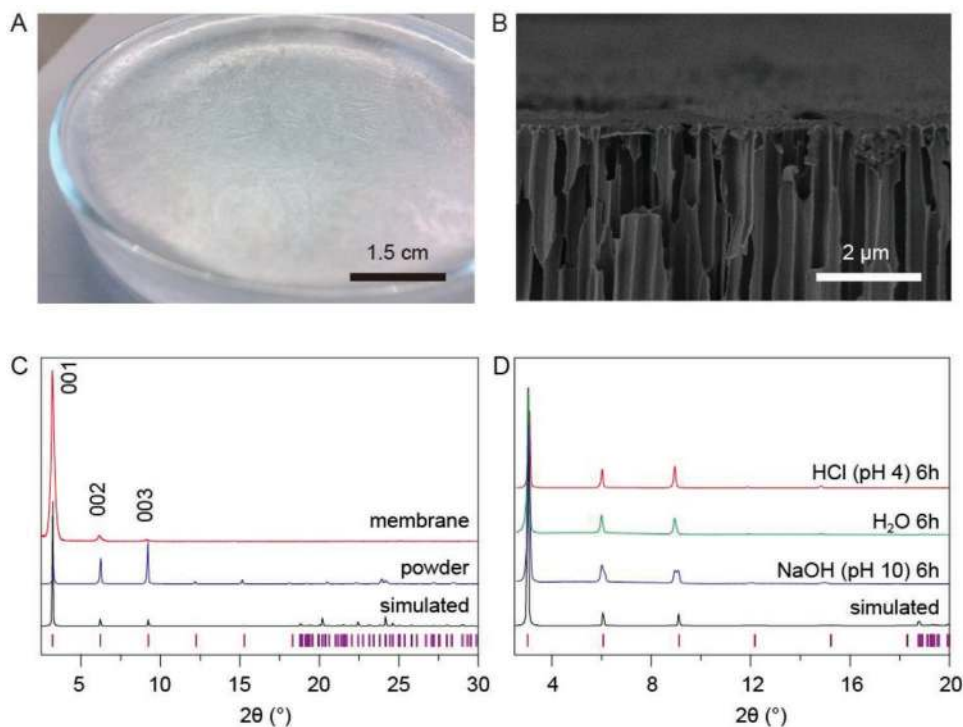


Figure 2. A) Image of CaC_{12} film floating on water. B) SEM cross-sectional view of CaC_{12} membrane on AAO with a pore size of 100 nm. C) XRD of CaC_{12} powder and membrane on AAO with a pore size of 100 nm. D) XRD of CaC_{12} powders after immersed in acidic and basic aqueous solutions for 6 h.

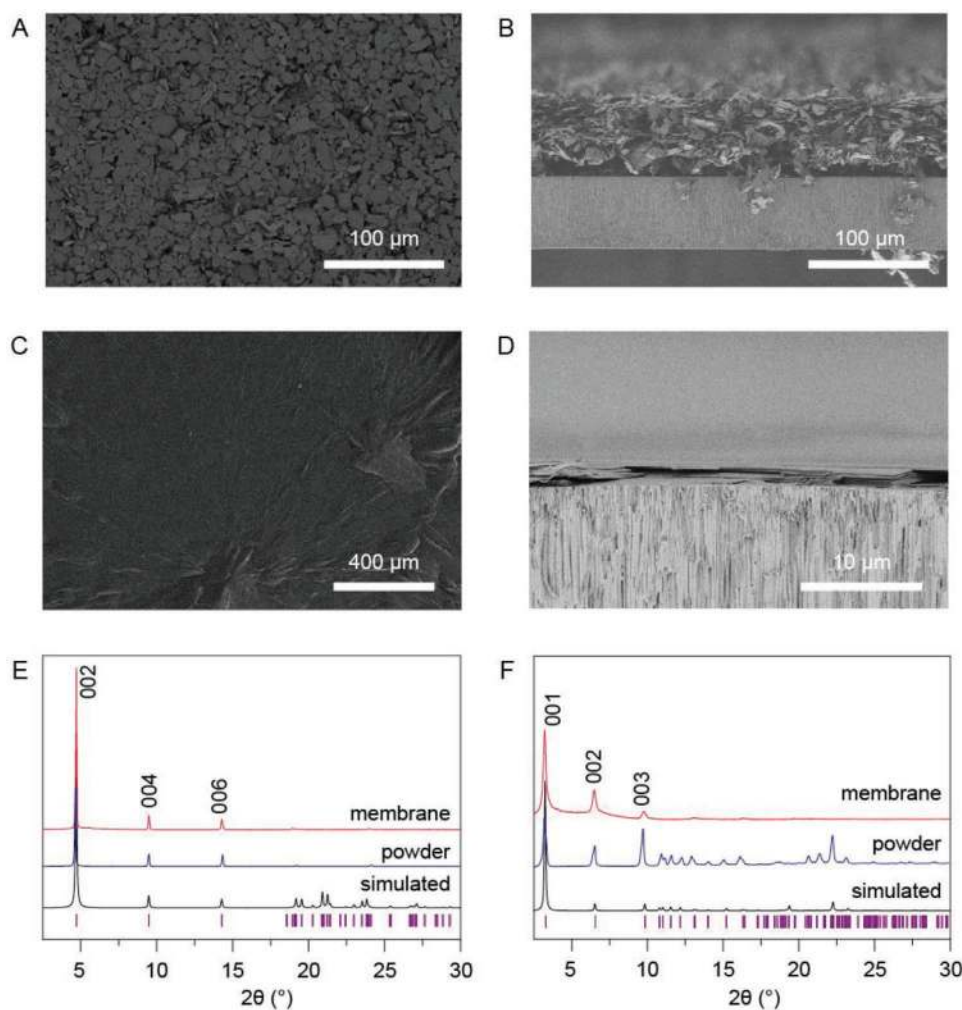


Figure 3. SEM images of the deposited ZnC₆ and as-synthesized membrane on AAO with a pore size of 100 nm: A,C) top view and B,D) cross-sectional view, respectively. E,F) XRD of as-synthesized powders and membranes: ZnC₆ and CuC₉.

For preparing ZnC₆ and CuC₉ membranes, we did not observe a similar film on the surface of the water. Therefore, we collected the precipitated metal soap crystals and prepared a suspension which was then vacuum filtered on to AAO substrates to form a deposit (Figures 1H and 3A, and Figure S7A, Supporting Information). Subsequently, the powder deposit was heated for a short time (150 °C and 40 min and 120 °C and 40 min for ZnC₆ and CuC₉, respectively) to obtain a melt. Finally, the molten film was cooled down to crystallize an intergrown membrane. Clogging of the AAO pores by the liquid melt was avoided to a large extent by flipping the AAO/powder assembly during heating (AAO at the top) exploiting the combined effect of the high viscosity of the liquid melt and gravity.

2.3. Characterizations of Metal Soap Membranes

Upon optimization of the deposition steps, we could prepare crack-free membranes for all three metal soaps. CaC₁₂ film prepared by the interfacial crystallization method led to an extremely thin and flexible membrane with a thickness

of ≈300 nm (Figure 2A,B, and Figures S2 and S17, Supporting Information). The grains in the film were quite large, exceeding tens of micrometers. As a result, the film was quite smooth and lacked textural features when viewed by the scanning electron microscope (SEM), atomic force microscope (AFM), and polarized optical microscope (POM) (Figure 2A, and Figures S2 and S17–S20, Supporting Information). As for ZnC₆ and CuC₉, the melts generated by heating the powders to a temperature above their melting points filled up the void spaces resulting in a highly dense structure (Figure 3C,D and Figure S7C,D, Supporting Information). The film thickness could be controlled by optimizing vacuum filtration conditions. In the present case, the average film thicknesses are 2 and 4 μm for ZnC₆ and CuC₉ films, respectively. These thicknesses are much less than that from the powders deposited on AAO before melting (60 and 20 μm for ZnC₆ and CuC₉ powders, respectively). From the cross-section images, it is clear that the pore channels of AAO are not clogged by the metal soap. Therefore, we avoided a problem that has been previously reported with the melting route (Figure 3D and Figure S7D, Supporting Information).^[43]

The crystallinity of the synthesized metal soap powders and the membranes was confirmed by XRD. The XRD patterns of three as-synthesized metal soap powders are almost identical to the simulated XRD patterns, indicating the phase purity of all three materials (Figures 2C, 3E, and 3F). Similarly, the XRD patterns showed high crystallinity for all three membranes (Figures 2C, 3E, and 3F). And the intensities of 00*l* peaks (001, 002, and 003 for CaC₁₂, 002, 004, and 006 for ZnC₆, and 001, 002, and 003 for CuC₉, respectively) from membranes were much higher compared to other peaks, which is in contrast to the simulated powder XRD patterns. This means the metal soap films are oriented on the substrate, with *c* axis perpendicular to the surface of the support. The stacking of layers is also evident in the cross-sectional SEM images of CaC₁₂ and ZnC₆ and transmission electron microscopy (TEM) image of CaC₁₂ membrane (Figure 3D, and Figures S2 and S16, Supporting Information). According to the crystal structures of the three membranes (Figure 1A,C,E), it is clear that all the alkyl chains are in a similar direction of channels from the substrates, which could favor gas transport.

The thermal and chemical stability of the metal soap powders were also investigated after the powders of CaC₁₂, ZnC₆, and CuC₉ were immersed in water, HCl (pH = 4), and NaOH (pH = 10) aqueous solutions for 6 h (Figure 2D, and Figures S8 and S9, Supporting Information). CaC₁₂ is stable in water and acid solutions. There are slight peaks splits around 6° and 9° of XRD after CaC₁₂ in NaOH solution for 6 h, indicating partially unit-cell distortions could have happened (Figure 2D), however, this does not hinder the application of CaC₁₂ in gas separation. ZnC₆ is stable in all solutions, and the XRD peaks maintained almost the same as the simulated pattern (Figure S8, Supporting Information). For CuC₉, the powder survived in water and acid solutions for 6 h. A small new peak around 5° of CuC₉ powder in HCl solution appeared after 6 h, indicating the structure could start to change (Figure S9, Supporting Information). Although these three structures are similar, the different metals and organic parts lead to different behavior in acid and basic solutions.

The stability of the prepared film in water was also studied, by immersing the films in water for 24 h, to understand the relevance of these membranes for application in separations involving liquid water. As shown in Figure S21 (Supporting Information), the morphology of the CuC₉ membrane is similar to that of the as-synthesized film. A comparison of the XRD data before and after the immersion test (Figure S22, Supporting Information) indicated that there were no changes in the film crystallinity, confirming the stability of CuC₉ membranes in water. However, water could delaminate CaC₁₂ immediately and the delaminated film floated on the surface of the water. ZnC₆ membranes also delaminated during the test. Thermogravimetric analysis (TGA) curves of CaC₁₂, ZnC₆, and CuC₉ in the air atmosphere showed they were thermally stable up to 150 °C (Figures S10, S11, and S12, Supporting Information), making them attractive for gas separation.

2.4. Gas Permeation Studies

Based on the crystal structure, the pore size relevant for the gas transport in the three metal soaps are approximately in the

range of 2.8–3.3 Å. In addition, the flexibility of alkyl chains in the structures is expected to provide some tolerance for gas transport. All indicate that these structures could be useful in light gas separations such as hydrogen sieving (H₂, kinetic diameter of 2.89 Å) or carbon capture (CO₂, kinetic diameter of 3.3 Å). N₂ adsorption isotherms of all three materials were collected at 77 K (Figures S13–S15, Supporting Information). All showed negligible uptake of N₂, which is consistent with the small pore sizes (2.8–3.3 Å) in these materials compared to the kinetic diameter of N₂ (3.64 Å). Accordingly, we tested the as-prepared crack-free membranes for gas separation.

The three metal soap films exhibited characteristically different permeation properties. The 300-nm-thick films of CaC₁₂ prepared by interfacial crystallization exhibited the highest gas permeance among the studied metal-soap films (Figure 4A,B; data based on five membranes). Single-component gas permeation studies at 25 °C revealed H₂ permeance of 6.1 × 10⁻⁷ mol m⁻² s⁻¹ Pa⁻¹ with an average H₂/N₂ and H₂/CH₄ selectivity of 4.4 and 5.5, respectively, which are higher than the corresponding Knudsen selectivities (3.7 and 2.8, respectively). However, CO₂ despite having a kinetic diameter of 3.3 Å exhibited the lowest permeance resulting in H₂/CO₂ selectivity as high as 10.5. This anomalous behavior is likely due to much stronger adsorption of CO₂ with the CaC₁₂ structure that may result from the strong bonding between Ca²⁺ and CO₂, where the bonding energy of Ca²⁺ and CO₂ is 8.0 kcal mol⁻¹, much larger than 4.6 kcal mol⁻¹ for Ca²⁺ and N₂.^[44] Similar behavior was also reported for 2D ZIF-L films.^[45] Considering the crystal structure of CaC₁₂, there are two kinds of pores with pore sizes 0.5 and 3.1 Å. Gas molecules cannot pass through the pores in the metal layers (0.5 Å) but they can transport across the gaps in the organic domain (3.1 Å). Because CaC₁₂ membranes are oriented on the support with the metal layers parallel to the surface of the support, gas molecules will inevitably pass the gaps between structure domains. This means Ca²⁺ ions on the edges of structural domains could attract CO₂, leading to the low CO₂ permeance in this membrane (Figure S30A, Supporting Information).

Gas transport studies from ZnC₆ membranes revealed H₂/CO₂, H₂/CH₄, and He/CH₄ ideal selectivities of 6.2, 11.3, and 5.6, respectively, at 25 °C (Figure 4C,D; data based on three membranes). These selectivities are significantly higher than the corresponding Knudsen selectivities (4.7, 2.8, and 2.0, respectively), and indicate separation based on molecular size with permeance in the order of H₂ > He > CO₂ > CH₄, with average H₂ permeance of 2.1 × 10⁻⁹ mol m⁻² s⁻¹ Pa⁻¹. The lower permeance of He with respect to H₂, despite the smaller size of He, can be explained by negligible heat of adsorption of He.^[46–48] The relative permeation rates depending on the kinetic diameter of gases in ZnC₆ membranes indicate transport dominated by diffusion. This has origin in its structure. Both pore sizes of metal layers and organic layers (2.8, 3.2, and 3.3 Å) are suitable for the transition of gases (especially for H₂). In addition, organic chains in ZnC₆ are the shortest compared to CaC₁₂ and CuC₉ (which means the structure of ZnC₆ could be more rigid than CaC₁₂ and CuC₉). Gas molecules could pass both the metal layers (for H₂) and gaps between structure domains (Figure S30B, Supporting Information).

The permeation characteristic of CuC₉ was different from that of CaC₁₂ and ZnC₆ membranes. With average CO₂

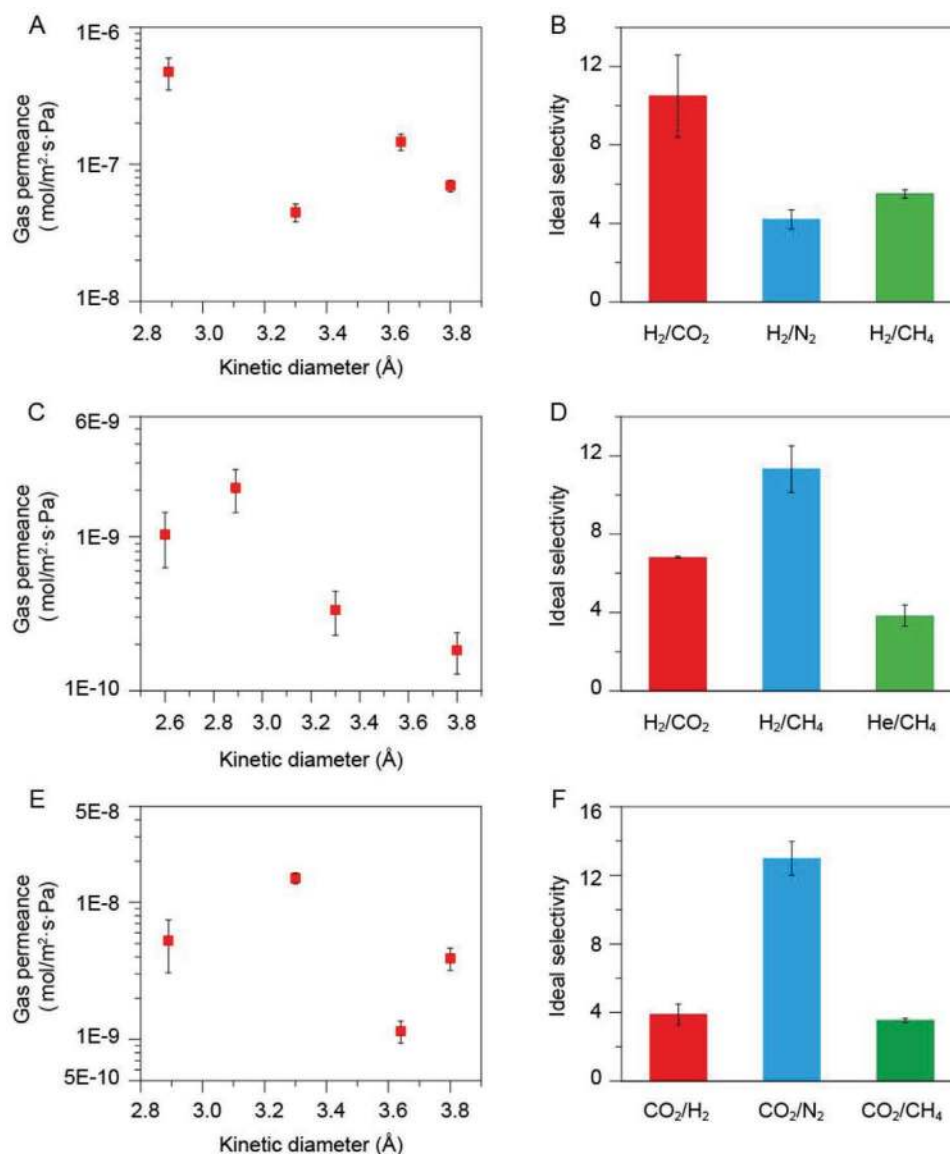


Figure 4. A,C,E) Gas permeances: CaC₁₂, ZnC₆, and CuC₉, and B,D,F) ideal selectivities of membranes: CaC₁₂, ZnC₆, and CuC₉, as a function of the kinetic diameters at 25 °C. Error bars in the figure represent the standard deviations across several membranes.

permeance of $1.5 \times 10^{-8} \text{ mol m}^{-2} \text{ s}^{-1} \text{ Pa}^{-1}$, CO₂ permeated faster than H₂ through the CuC₉ membrane. An attractive CO₂/N₂ ideal selectivity of 13.6 was realized. CO₂ permeance did not change when the feed was pressurized from 1.5 to 3 bar, although the CO₂/N₂ ideal selectivity decreased slightly to 10.7 (Figure S24, Supporting Information). When an equimolar CO₂/N₂ feed was used, CO₂ permeance did not change while the CO₂/N₂ separation factor was 12.2 at feed pressure of 3.0 bar (Figure S25, Supporting Information). The transport of CO₂ was thermally activated, and CO₂ permeance increased when the temperature was increased from 25 to 75 °C (Figure S26, Supporting Information). When the temperature was increased to 100 °C, close to the melting temperature of CuC₉, permeances of CO₂ and N₂ decreased a little perhaps attributing to possible structural changes near the melting point.

By decreasing the amount of CuC₉ powders filtered on the substrate before melting, an extremely thin ($\approx 250 \text{ nm}$) yet continuous CuC₉ membrane could be obtained (Figure S27, Supporting Information). The CO₂/N₂ ideal selectivity was 5.5–6.4, much above the Knudsen selectivity indicating that pinhole defects in the film were negligible (Figure S28B, Supporting Information). The CO₂ permeance from this membrane was about $6.2 \times 10^{-8} \text{ mol m}^{-2} \text{ s}^{-1} \text{ Pa}^{-1}$, four times higher than the thicker membrane reported above (Figure S28A, Supporting Information). The gain in CO₂ permeance was not as high as expected, where the film thickness was decreased by 16-fold, which could be attributed to infiltration of CuC₉ in the support pores during melting. The separation performance from mixed feed (equimolar CO₂/N₂) was similar to that obtained from the single component (Figure S29A, Supporting Information), and the performance did not change as a function of time

(Figure S29B, Supporting Information). Mixing feed with the water vapor close to saturation also did not affect the performance (Figure S29C, Supporting Information).

Similar to what is commonly observed with a number of nanoporous polymers (polymers with intrinsic microporosity or PIM, poly[1-(trimethylsilyl)-1-propyne or PTMSP, polydimethylsiloxane, etc.),^[49–54] the single-component gas permeance for CuC₉ decreased in the order CO₂ > H₂ > CH₄ > N₂ with CO₂/H₂, CO₂/CH₄, and CO₂/N₂ selectivities of 2.9, 3.9, and 13, respectively (Figure 4E,F, based on two membranes). The 1D rod-like structures of CuC₉ are similar to polymer chains which might explain the similar permeation characteristics.

In all, although these three materials are all metal soaps, their behaviors in gas permeations are different, attributing to their unique structure and chemical composition. ZnC₆ membranes appear to separate molecules based on their size, CuC₉ membranes similar to nanoporous polymers with a high permeation rate of CO₂, while CaC₁₂ membranes inhibit the permeation rate of CO₂. The diverse gas separation performance indicates that metal soap membranes can act as flexible polymers as well as rigid nanoporous materials, attributing to their rich diversity of structures, which contain both long carbon chains and bonding of metal cations and functional groups, and are highly crystalline at the same time.

Compared to the recent reports of MOF glass membranes,^[43] metal soaps retain their crystallinity in the final membrane structure. It should be noted that the melting points of metal soaps are much lower than that of MOFs (about 100–200 °C vs 400 °C). The facile processability of the metal soap membranes prepared either by the simple interfacial crystallization technique or by the melting method and a large number of potentially interesting structures, make them an interesting class of materials for molecular separation.

3. Conclusion

In conclusion, we report for the first time, the synthesis of crack and defect-free metal soap membranes and their application in gas separation. The rapid interfacial crystallization and the melting methods demonstrated here add to the ongoing efforts to rapidly synthesize crystalline nanoporous films to improve their scale-up potential. The diverse structure of metal soaps is reflected in their gas separation behavior leading to performance resembling nanoporous materials as well as polymeric chains, attributing to the presence of inorganic layers as well as organic channels in the metal soaps. There are many more possibilities of metal soaps depending upon the combination of metal cation, surfactant chain length, and the functional group of the surfactant.

4. Experimental Section

The syntheses of metal soap powders were carried out by a slight adaptation of the method reported in the literature.^[37,41,42] For CaC₁₂, 2.36 g Ca(NO₃)₂·4H₂O and 5.76 g SDS were dissolved in 10 mL deionized water, respectively. A white precipitate formed immediately after the two solutions were mixed. For ZnC₆, 2.97 g Zn(NO₃)₂·6H₂O was dissolved in 10 mL deionized water. A mixture of 2.60 g heptanoic acid and 0.8 g NaOH was also dissolved in 10 mL deionized water. The two solutions

were then mixed, and a white precipitate appeared in few seconds. For CuC₉, 2.41 g Cu(NO₃)₂·3H₂O was dissolved in 10 mL deionized water. A mixture of 3.44 g decanoic acid and 0.8 g NaOH was also dissolved in 10 mL deionized water. Then the two solutions were mixed to get blue precipitate in a few seconds. In all cases, the precipitate was filtered and washed with water. The powder was obtained by drying in air overnight. For the synthesis of CaC₁₂ membrane, 5 mL of 0.1 M of SDS was added dropwise into 10 mL of 0.1 M Ca(NO₃)₂ aqueous solution. Once the whole water surface was covered, the film was scooped using a suitable porous substrate. Several kinds of porous substrates were used including AAO hosting 100 and 20 nm pores, porous PTFE membranes with pore sizes of 300 nm, and a metal mesh with pore sizes of 5 μm. All membranes were dried overnight under the ambient conditions. Both ZnC₆ and CuC₉ membranes were synthesized by the following recipe: At first, 10 mg of ZnC₆ or CuC₉ powders were dispersed in 20 mL deionized water by ultrasonication for 30 min. 2 mL of the suspension was subsequently vacuum-filtered on AAO hosting 100 nm pores. Finally, the ZnC₆ or CuC₉ powder on AAO was heated at high temperatures for a fixed time (150 °C and 40 min for ZnC₆ and 120 °C and 40 min for CuC₉, respectively), and then cooled down slowly to form the membranes.

Supporting Information

Supporting Information is available from the Wiley Online Library or from the author.

Acknowledgements

The authors acknowledge the host institution, EPFL, for the generous support. This work was supported by European Research Council Starting Grant (805437-UltimateMembranes) and Swiss National Science Foundation Assistant Professor Energy Grant (PYAPP2_173645). The authors thank Prof. Bourban Pierre-Etienne from DLL-STI-GE, EPFL for the POM measurement, Dr. Mehrdad Asgari from LFIM, EPFL for the N₂ adsorption test, and Dr. Andrea Cerreta and Dr. H. Jens Böttcher from Park Systems Europe GmbH for the AFM measurement. Special thanks to all the group members' support and help in LAS group.

Conflict of Interest

The authors declare no conflict of interest.

Keywords

gas separation, interfacial crystallization, melting, membranes, metal soaps

Received: July 6, 2020
Revised: August 30, 2020
Published online:

- [1] N. Rangnekar, N. Mittal, B. Elyassi, J. Caro, M. Tsapatsis, *Chem. Soc. Rev.* **2015**, *44*, 7128.
- [2] B. Seoane, J. Coronas, I. Gascon, M. Benavides, O. Karvan, O. J. Caro, F. Kapteijn, J. Gascon, *Chem. Soc. Rev.* **2015**, *44*, 2421.
- [3] F. Yang, F. Tao, C. Li, L. Gao, P. Yang, *Nat. Commun.* **2018**, *9*, 5443.
- [4] A. Huang, Q. Liu, N. Wang, Y. Zhu, J. Caro, *J. Am. Chem. Soc.* **2014**, *136*, 14686.
- [5] H. Park, J. Kamcev, L. Robeson, M. Elimelech, B. Freeman, *Science* **2017**, *356*, 307.
- [6] W. Koros, C. Zhang, *Nat. Mater.* **2017**, *16*, 289.

- [7] L. Wang, M. Boutilier, P. Kidambi, D. Jang, N. Hadjiconstantinou, R. Karnik, *Nat. Nanotechnol.* **2017**, *12*, 509.
- [8] H. Li, Z. Song, X. Zhang, Y. Huang, S. Li, Y. Mao, H. Ploehn, Y. Bao, M. Yu, *Science* **2013**, *342*, 95.
- [9] L. Prozorovska, P. R. Kidambi, *Adv. Mater.* **2018**, *30*, 1801179.
- [10] K. Xie, Q. Fu, C. Xu, H. Lu, Q. Zhao, R. Curtain, D. Gu, P. Webley, G. Qiao, *Energy Environ. Sci.* **2018**, *11*, 544.
- [11] Z. Qiao, S. Zhao, M. Sheng, J. Wang, S. Wang, Z. Wang, C. Zhong, M. Guiver, *Nat. Mater.* **2019**, *18*, 163.
- [12] J. Wei, Y. Hu, Y. Liang, B. Kong, J. Zhang, J. Song, Q. Bao, G. Simon, S. Jiang, H. Wang, *Adv. Funct. Mater.* **2015**, *25*, 5768.
- [13] F. Wang, P. Carbone, R. Joshi, R. Nair, A. Geim, A. H. Wu, Y. Su, I. Grigorieva, V. Kravets, *Science* **2014**, *343*, 752.
- [14] M. Pera-Titus, *Chem. Rev.* **2014**, *114*, 1413.
- [15] K. Agrawal, B. Topuz, T. Pham, T. Nguyen, N. Sauer, N. Rangnekar, H. Zhang, K. Narasimharao, S. Basahel, L. Francis, C. Macosko, S. Al-Thabaiti, M. Tsapatsis, K. Yoon, *Adv. Mater.* **2015**, *27*, 3243.
- [16] H. Zhang, Q. Xiao, X. Guo, N. Li, P. Kumar, N. Rangnekar, M. Jeon, S. Al-Thabaiti, K. N. Rao, S. Basahel, B. Topuz, F. Onorato, C. Macosko, A. Mkhoyan, M. Tsapatsis, *Angew. Chem. Int. Ed.* **2016**, *55*, 7184.
- [17] A. Brown, N. Brunelli, K. Eum, F. Rashidi, J. Johnson, W. Koros, C. Jones, S. Nair, *Science* **2014**, *345*, 72.
- [18] C. Kong, H. Du, L. Chen, B. Chen, *Energy Environ. Sci.* **2017**, *10*, 1812.
- [19] G. He, M. Dakhchoune, J. Zhao, S. Huang, K. Agrawal, *Adv. Funct. Mater.* **2018**, *28*, 170742.
- [20] D. Babu, G. He, J. Hao, M. Vahdat, P. Schouwink, M. Mensi, K. Agrawal, *Adv. Mater.* **2019**, *31*, 1900855.
- [21] D. Babu, G. He, L. F. Villalobos, K. V. Agrawal, *ACS Sustainable Chem. Eng.* **2019**, *7*, 49.
- [22] X. Ma, P. Kumar, N. Mittal, A. Khlyustova, P. Daoutidis, K. Mkhoyan, M. Tsapatsis, *Science* **2018**, *361*, 1008.
- [23] D. Shinde, G. Sheng, X. Li, M. Ostwal, A. Emwas, K. Huang, Z. Lai, *J. Am. Chem. Soc.* **2018**, *140*, 14342.
- [24] S. Kandambeth, B. Biswal, H. Chaudhari, K. Rout, H. Kunjattu, S. Mitra, S. Karak, A. Das, R. Mukherjee, U. Kharul, R. Banerjee, *Adv. Mater.* **2017**, *29*, 1603945.
- [25] H. Fan, J. Gu, H. Meng, A. Knebel, J. Caro, *Angew. Chem. Int. Ed.* **2018**, *57*, 4083.
- [26] C. Zhang, B. Wu, M. Ma, Z. Wang, Z. Xu, *Chem. Soc. Rev.* **2019**, *48*, 3811.
- [27] H. Yang, L. Yang, H. Wang, Z. Xu, Y. Zhao, Y. Luo, N. Nasir, Y. Song, H. Wu, F. Pan, Z. Jiang, *Nat. Commun.* **2019**, *10*, 2101.
- [28] J. Hao, D. J. Babu, Q. Liu, H.-Y. Chi, C. Lu, K. V. Agrawal, *J. Mater. Chem. A* **2020**, *8*, 7633.
- [29] G. Klimusheva, T. Mirnaya, Y. Garbovskiy, *Liq. Cryst. Rev.* **2015**, *3*, 28.
- [30] R. Corbery, *Curr. Opin. Colloid Interface Sci.* **2008**, *13*, 288.
- [31] J. Peultier, E. Rocca, J. Steinmetz, *Corros. Sci.* **2003**, *45*, 1703.
- [32] J. Peng, G. Barnes, I. Gentle, *Adv. Colloid Interface Sci.* **2001**, *91*, 163.
- [33] A. Zapf, R. Beck, G. Platz, H. Hoffmann, *Adv. Colloid Interface Sci.* **2003**, *100*, 349.
- [34] M. Zhou, P. R. Nemade, X. Lu, X. Zeng, E. S. Hatakeyama, R. D. Noble, D. L. Gin, *J. Am. Chem. Soc.* **2007**, *129*, 9574.
- [35] D. Blunk, K. Praefcke, V. Vill, *Handbook of Liquid Crystals*, Wiley-VCH, Weinheim, Germany **1998**.
- [36] S. Tavares, F. Wypych, A. Letao, *Chem. Phys. Lett.* **2015**, *636*, 154.
- [37] M. Riesco, F. Martinez-Casado, J. Cheda, I. Yelamos, I. Silva, T. Plivelic, S. Lopez-Andres, P. Ferloni, *Cryst. Growth Des.* **2015**, *15*, 2005.
- [38] R. Miller, J. Cabral, E. Robles, N. Brookes, O. Ces, *CrystEngComm* **2018**, *20*, 6834.
- [39] A. Maneedaeng, A. Flood, B. Grady, K. Haller, *Cryst. Growth Des.* **2011**, *11*, 2948.
- [40] V. Luzzati, A. Tardieu, T. Gulik-Krzywicki, E. Rivas, F. Reiss-Husson, *Nature* **1968**, *220*, 485.
- [41] G. Sakane, M. Tomohara, Y. Katayama, K. Hayashi, *Acta Crystallogr.* **2010**, *E66*, 749.
- [42] F. Lacouture, J. Peultier, M. Francois, J. Steinmetz, *Acta Crystallogr.* **2000**, *C56*, 556.
- [43] Y. Wang, H. Jin, Q. Ma, K. Mo, H. Mao, A. Feldhoff, X. Cao, Y. Li, F. Pan, Z. Jiang, *Angew. Chem. Int. Ed.* **2020**, *59*, 4365.
- [44] R. G. Keese, A. W. Castleman, *J. Chem. Phys. Ref. Data* **1986**, *15*, 1011.
- [45] Z. Zhong, J. Yao, R. Chen, Z. Low, M. He, J. Z. Liu, H. Wang, *J. Mater. Chem. A* **2015**, *3*, 15715.
- [46] W. A. Steele, J. G. Aston, *J. Am. Chem. Soc.* **1957**, *79*, 2393.
- [47] B. J. Schindler, M. D. LeVan, *Carbon* **2008**, *46*, 644.
- [48] E. L. Pace, A. R. Siebert, *J. Phys. Chem.* **1960**, *64*, 961.
- [49] M. Carta, R. Malpass-Evans, M. Croad, Y. Rogan, J. C. Jansen, P. Bernardo, F. Bazzarelli, N. B. McKeown, *Science* **2013**, *339*, 303.
- [50] C. G. Bezzu, M. Carta, A. Tonkins, J. C. Jansen, P. Bernardo, F. Bazzarelli, N. B. McKeown, *Adv. Mater.* **2012**, *24*, 5930.
- [51] Q. Song, S. Cao, P. Zavala-Rivera, L. P. Lu, W. Li, Y. Ji, S. A. Al-Muhtaseb, A. K. Cheetham, E. Sivaniah, *Nat. Commun.* **2013**, *4*, 1918.
- [52] M. Carta, M. Croad, R. Malpass-Evans, J. C. Jansen, P. Bernardo, G. Clarizia, K. Friess, M. Lanc, N. B. McKeown, *Adv. Mater.* **2014**, *26*, 3526.
- [53] A. M. Shishatskiy, S. Wind, J. Zhang, X. Nottbohm, C. T. Mellech, N. A. Winter, H. Vieker, J. Qiu, K. J. Dietz, A. Götzhäuser, A. Beyer, *Adv. Mater.* **2014**, *26*, 3421.
- [54] S. Li, Z. Wang, X. Yu, J. Wang, S. Wang, *Adv. Mater.* **2012**, *24*, 3196.